PHYSICAL CHEMISTRY OF NANOCLUSTERS AND NANOMATERIALS

Pure and Cu-Doped ZnO Nanoparticles: Hydrothermal Synthesis, Structural, and Optical Properties

L. Ben Saad[a], L. Soltane[a], and F. Sediri[a,b],*

[a] *Unité de Recherche de Matériaux et Environnement (UR15ES01), IPEIT, Université de Tunis,*
2 Rue Jawaher Lel Nehru, Montfleury, 1089 Tunisia
[b] *Faculté des Sciences de Tunis, Université de Tunis El Manar, El Manar Tunis, 2092 Tunisia*
* e-mail: faouzi.sediri@fst.utm.tn

Abstract—Pure and Cu-doped zinc oxide ($Zn_{1-x}Cu_xO$ with $x = 0.00$, 0.05, 0.10, and 0.15) nanoparticles were prepared via hydrothermal synthesis using a solution of zinc sulfate ($ZnSO_4$) as precursor, *p*-phenylenediamine as structure-directing agent in the presence of different amounts of $CuSO_4$ and NaOH. XRD, Raman, UV–Vis, and PL techniques were used to characterize the as-synthesized samples. The XRD analysis reveals that the average particle size of pure ZnO is 13.50 nm. It decreased to 12.11 nm for the Cu-doped sample $Zn_{0.95}Cu_{0.05}O$, then to 11.00 nm when $x = 0.15$ ($Zn_{0.85}Cu_{0.15}O$). The optical band gap of pure and Cu-doped ZnO nanoparticles was calculated from UV–Vis spectra. It turned out to have decreased from 3.18 to 3.11 eV as the amount of Cu increases up from $x = 0$ to 0.15. The photoluminescence study shows that the introduction of Cu into pure ZnO causes a decrease in surface defects, such as oxygen vacancy and zinc vacancy.

INTRODUCTION

The semiconductor nanomaterials are of great interest. They have attracted much research in recent years because of their possible applications in the fields of such as gas sensors [1], solar cells [2], field-effect transistors (FETs) [3], electronics and optoelectronics [4, 5]. One of the most desired semiconductors is zinc oxide ZnO which is an *n*-type II–VI semiconductor most stable when crystallized in wurtzite structure. In fact, it is a semiconductor with a large direct gap (the energy gap between the valence band and the conduction band is 3.37 eV) [6]. It plays a major role in the development of new applications in photonics. For example, it is a good candidate for transparent electrical contacts in the visible spectral range (surface electrodes of solar panels). It is also used in manufacturing lasers emitting in the blue or near ultraviolet light. ZnO is also comparable with other large band gap semiconductors, such as SiC and GaN [7]. In addition, the high binding energy of the free exciton of ZnO (about 60 meV) [8, 9] and its high melting point (2250 K) make it potentially very effective in excitonic emission devices, as this gives it good high temperature operating stability and makes it a better material than GaN. However, the essential lock of ZnO is to obtain stable and reproducible *p*-type doping. This obstacle significantly hinders the development of ZnO technology for optoelectronic components.

Currently, scientific researchers are interested in the application of ZnO as a photocatalyst for the degradation of organic pollutants, such as dyes, due to photosensitivity of a non-toxic material and chemical stability [10–12]. Several studies have shown that the incorporation of certain dopants, such as transition metals and rare earths in semiconductor oxides can improve their optical, structural, and photocatalytic properties [13, 14]. Indeed, doping causes the appearance of new acceptor levels and electron donors in the band structure of the doped material. These levels appear in the gap, between the conduction band and the valence band [15, 16].

For the last few years, several studies on ZnO doping have already been carried out on thin layers or massive. Except for the works of Tsukazaki et al. [17] who had successfully prepared ZnO-based LED, the other obtained results are often unconvincing or not reproducible. Crystalline defects, impurities and self-compensation phenomena remain high and limit the realization of *p*-type ZnO. Several methods have been used to prepare Cu-doped ZnO, such as pulsed laser deposition (PLD) and chemical vapor deposition (CVD), which require relatively high temperatures [18–20]. Copper-doped ZnO nanorods, were elaborated by hydrothermal method without annealing treatment [21].
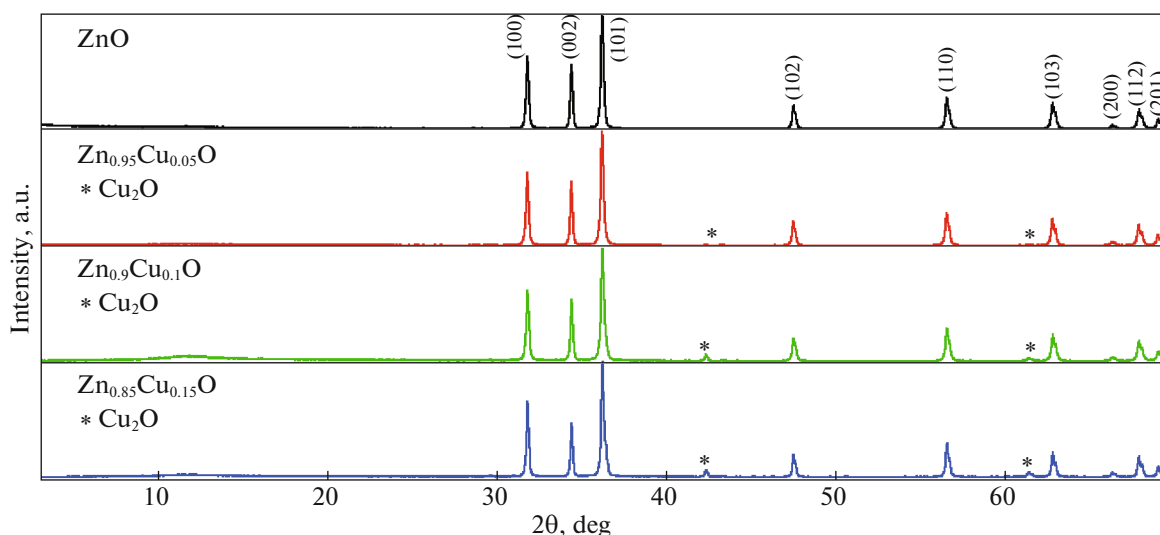
Fig. 1. (Color online) XRD patterns of undoped and Cu-doped ZnO.

This paper deals with the hydrothermal synthesis, in simple one-step, without post-annealing of Cu-doped ZnO nanoparticles. The study of their optical properties was also reported. Although many methods have been developed to elaborate copper doped zinc oxide nanoparticles, to the best of our knowledge, this is the first report of Cu-doped ZnO nanoparticles synthesis using zinc sulfate and p-phenylenediamine as structure-directing agent.

EXPERIMENTAL

The synthesis of pure nanorods ZnO was performed using zinc sulfate (0.532 g), p-phynelynediamine (0.200 g), and sodium hydroxide (0.735 g). All reagents were mixed in order in 10 mL of distilled water under agitation for one hour at room temperature. The pH of the reaction mixture was maintained as 14. The aqueous solution was placed in a steel autoclave coated with Teflon in an oven for 4 h at 180°C. The obtained powder was washed several times with distilled water and ethanol to remove organic residues and finally dried for 4 h at 80°C.

For the preparation of $Zn_{1-x}Cu_xO$ nanoparticles, zinc sulfate was mixed with copper sulfate, sodium hydroxide and p-phenylendiamine, whose amounts are indicated above, dissolved in 10 mL distilled water and kept on magnetic stirrer for 1 h under vigorous stirring. Then it underwent a 4-h hydrothermal treatment at 180°C. The obtained precipitate was separated from the solution and washed several times with distilled water and ethanol to remove any unreacted precursors. It was then dried at 80°C for 4 h. In order to study the effect of doping on the optical properties, we

have varied the value of x as follows $x = 0.00, 0.05, 0.10,$ and 0.15.

The X-ray powder diffraction data (XRD) were obtained on a X'Pert Pro Panalytical diffractometer with CuK_α radiation ($\lambda = 1.5406$ Å) and graphite monochromator. The XRD measurements were carried out by a step scanning method (2θ range from 3° to 70°), the scanning rate is 0.01 s^{-1} and the step time is 15 s. Raman spectroscopy was performed using a Jobin Yvon T 64000 spectrometer (blue laser excitation with 488 nm wavelength and <55 mW power at the sample). UV–Vis spectra were recorded on Shimadzu UV3101PC Visible spectrophotometer in the wavelength range of 200−800 nm. The photoluminescence (PL) measurements have been carried out using a Jobin Yvon luminescence spectrometer at the excitation wavelength of 325 nm.

RESULTS AND DISCUSSION

Phase Structure

The XRD patterns of the as-prepared pure ZnO and Cu-doped ZnO nanparticles ($Zn_{1-x}Cu_xO$ with $x = 0, 0.05, 0.1,$ and 0.15) are shown in Fig. 1. The well-defined diffraction peaks in the XRD diagram clearly shows the crystalline character with peaks corresponding to (100), (002), (101), (102), (110), (103), (200), (112), and (201) planes according to the standard JCPDS card no. 89-7102 and is indexed as the hexagonal wurtzite with preferred orientation along (101) plane in all the samples.

According to XRD patterns, the additional Cu$_2$O peak is observed in the doped samples. In fact, the XRD patterns of the samples $Zn_{1-x}Cu_xO$ ($x = 0.05, 0.1,$ and 0.15) show the presence of all ZnO diffraction peaks at the same time with a slight shift in the 2θ posi-

tions and the presence of additional peaks at $2\theta = 29.64°$, $42.40°$, and $61.46°$ which are related to the planes (110), (200), and (220) of Cu_2O phase with cubic structure (JCPD no. 77-0199). Generally, when it comes to the incorporation of the Cu^{2+} ion, the diffraction peak intensity (002) of Cu-doped ZnO decreases with increasing Cu concentration, but their total width at the half of the maximum FWHM increases**,** and this can be explained by a degradation of the crystallographic characteristics of Cu doped ZnO and a shift in the position of the main peaks. So, in our case, this suggests that this is a substitution of Zn^{2+} (0.074 nm) by Cu^{2+} (0.072 nm) [22, 23].

The average crystallite size (L) of the as-synthesized samples was estimated by using Scherrer's formula:

$$L = \frac{0.89\lambda}{\beta\cos\theta},$$

where L is the average crystallite size, $\lambda = 1.5406$ Å, β is the half maximum peak width, and θ is the diffraction angle in degrees [24]. The average crystallite sizes of pure and Cu-doped ZnO calculated from XRD patterns was found to be about $11-13$ nm (Table 1).

The lattice constants a and c for hexagonal wurtzite ZnO nanopowders are also estimated from the equation [25]:

$$a = \frac{\lambda}{2\sin\theta}\sqrt{\frac{4}{3}(h^2 + hk + k^2) + \frac{l^2}{(c/a)^2}}$$

and

$$c = \frac{\lambda}{2\sin\theta}\sqrt{\frac{4}{3}\left(\frac{(h^2 + hk + k^2)}{(a/c)^2}\right) + l^2}.$$

Therefore, the analysis of the results reveals that the average values of a and c parameters are 0.3249 and 0.5209 nm, respectively.

Optical Properties

The UV–Vis absorption spectra of the as-synthesized undoped and Cu-doped ZnO nanoparticles are shown in Fig. 2. It is obvious that all the samples show a strong absorption in the ultraviolet region near the visible-light region, demonstrating that the obtained ZnO samples have better UV absorption. In fact, the pure ZnO spectrum has a characteristic absorption band at 400 nm. However, absorption spectra of Cu-doped ZnO show an offset of the absorption band at a lower wavelength about 396 nm than that of pure ZnO. This phenomenon suggests that the incorporation of Cu into ZnO causes a decrease in the absorption band. Consequently, the absorption edge shifts towards lower wavelength with the increase of Cu content in ZnO.

The typical room temperature transmittance spectra for undoped ZnO and different Cu doped ZnO are

Table 1. Crystallite size (d) and average lattice parameter (a, c) of as-synthesized undoped and Cu-doped ZnO nanoparticles

| Samples	d, nm	a, nm	c, nm
ZnO	13.05	0.3250	0.5673
$Zn_{0.95}Cu_{0.05}O$	12.11	0.3251	0.5673
$Zn_{0.9}Cu_{0.1}O$	11.75	0.3250	0.5671
$Zn_{0.85}Cu_{0.15}O$	11.00	0.3250	0.5671

shown in Fig. 3. The transmission spectra of the Cu doped ZnO nanoparticles show just the opposite trend of the optical absorption spectra. The transmittance spectra reveal that pure ZnO has a 50% increased reflectance compared to Cu-doped ZnO samples which are decreased by increasing the Cu concentration in ZnO [26]. The optical band energy was calculated by extrapolation of the linear part of plot between the $(\alpha h\nu)^2$ vs. $h\nu$ (Fig. 2). The band gap values of pure ZnO and $Zn_{0.95}Cu_{0.05}O$ are nearly identical and found to be 3.18 and 3.14 eV, respectively. For $Zn_{0.90}Cu_{0.1}O$ and $Zn_{0.85}Cu_{0.15}O$ there is a slight offset of 0.02 eV which are 3.13 and 3.11 eV, respectively. The band gap values decreases slightly from 3.18 to 3.11 eV (almost constant) when the amount of Cu (x) ranged from 0 to 0.15. This may confirm the substitution of Cu^{2+} by Zn^{2+} [27]. Regarding Cu-doped ZnO nanoparticles samples, it was found that the band gap decreased by increasing the dopant content, which is similar to the results reported by Labhane et al. [28]. The systematic decrease in the band gap could not be due to the structural changes by adding Cu into ZnO. The reduction of gap energy could not be due to structural modifications resulting from the addition of Cu in the ZnO matrix. Indeed, since Cu and Zn are neighbors in the periodic table, they do not obviously modify the crystal structure when they are replaced, as shown by our XRD study.

The detected red shift in the gap energy ($\Delta E_g = 0.07$ eV) can be explained by the doping phenomenon. An analogue decrease in the band gap was also observed. It can be explained by the $p-d$ interactions of the spin swap between the band electrons and the localized d one of the transition metal ion replacing the Cu^+ [29, 30]. Theoretically, using the second-order perturbation theory, this phenomenon has been explained by the exchange interactions $s-d$ and $p-d$ [31]. They revealed that this shift asserts (confirms) the uniform substitution of Cu^{2+} ions in the ZnO lattice. Furthermore, the effects of many bodies on the conduction and valence bands could be the cause of the reduction of the forbidden band [31], which can reduce this band and result from the electron interaction and diffusion of impurities. This has been assigned to the fusion of a band of impurities with a
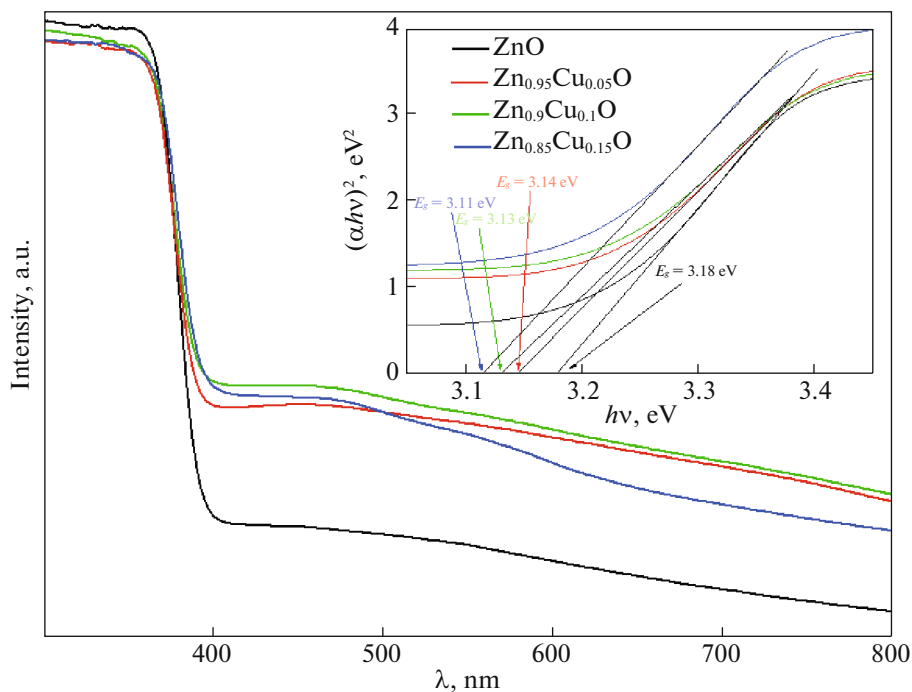
Fig. 2. (Color online) UV–Vis absorption spectra and the $(\alpha h\nu)^2$ vs. $h\nu$ plot (insert) of undoped and Cu-doped ZnO.
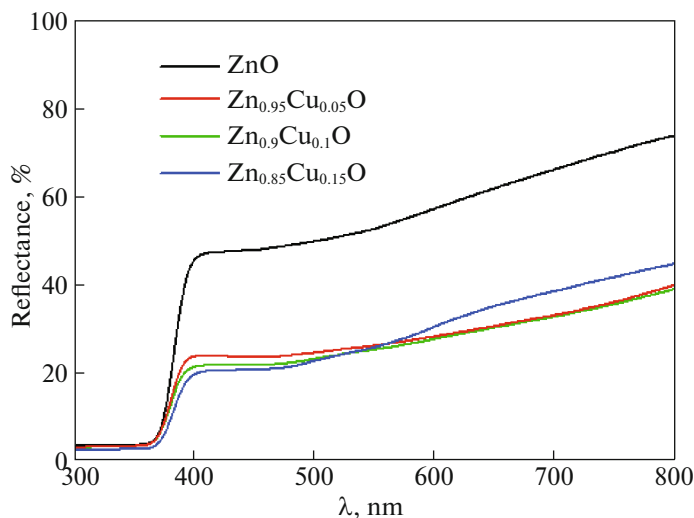
Fig. 3. (Color online) Reflexctance spectra of undoped and Cu-doped ZnO.

conduction band, which, in turn, led to the reduction of band gap.

A photoluminescence study was carried out at room temperature in order to study the optical properties and the effects of Cu doping in ZnO. PL spectra of pure and Cu-doped ZnO with different amounts of Cu are illustrated on Fig. 4. All the spectra exhibit an excitonic peak in ultraviolet region and defect related peak in the visible region which is essentially related to ZnO defects. All samples exhibit a peak around 398 nm associated with near band ultra violet emission. This ultra violet band corresponds to the near band-edge (NBE) emission, which is related essentially to the recombination of free excitations [32–34].

A strong blue band at 460 nm was also observed for all samples with a slight offset for pure ZnO. In addition, the spectra show a weak blue-green emission peaks around 490 and 530 nm [35]. For undoped ZnO
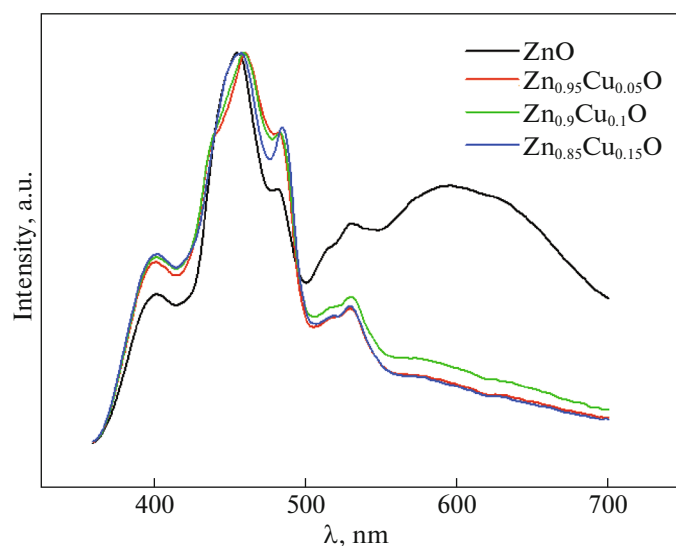
Fig. 4. (Color online) Room temperature PL spectra of undoped and Cu-doped ZnO.
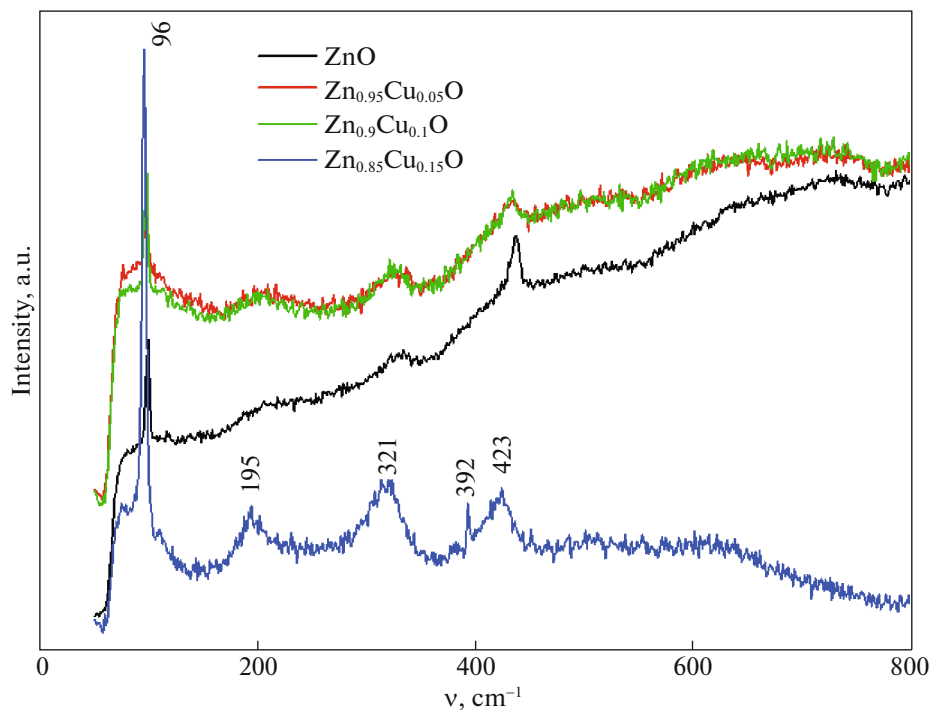

Fig. 5. (Color online) Raman spectra of undoped and Cu-doped ZnO.

another broad deep-level emission (DLE) was observed at 595 nm (yellow and orange emission), which is usually attributed to the ionized oxygen vacancies [36]. There is a decrease in the intensity of the green band at 530 nm and that of the orange band at 595 nm for Cu-doped ZnO samples compared to pure ZnO. Therefore, the introduction of Cu into ZnO matrix causes a decrease in surface defects, such

as oxygen vacancy and zinc vacancy [37], thus, increasing the copper content during the doping process reduces the optical quality of ZnO.

The Raman spectroscopy technique is essential and allows determining the perfection of crystals and structural defects. Hexagonal wurtzite ZnO structure with space group $C_{6v}^4(P_3^6mc)$ is characterized by two formula units in the primitive cell [38, 39]. According

to group theory, the following optical modes are expected: $A_1 + 2B_1 + E_1 + 2E_2$, whereabouts A_1, E_1, and E_2 are the first order Raman active modes, and B_1 is forbidden [40]. Figure 5a shows the Raman spectrum of as synthesized undoped ZnO. The characteristic peak of the E_2 (high) mode at 438 cm^{-1} represents wurtzite hexagonal structure of ZnO. The two peaks located at 330 and 382 cm^{-1} can be assigned to the $E_{2H}-E_{2L}$ and A_1 (TO) modes, respectively [41]. Figures 5b−5d display the Raman spectra of Cu-doped ZnO nanoparticles with a variable amount of copper. For all doped samples, the presence of the main peak in E_2 mode (high) is observed around 427 cm^{-1} with another peak located at 318 cm^{-1} attributed to the $E_{2H}-E_{2L}$ mode.

The spectral analysis revealed that when the Cu doping concentration increases, the maximum intensities decrease with the disappearance of the A_1 (TO) mode, which suggests that the ZnO bond breakdown changes with Cu doping. TO and LO are optical phonons, respectively transversal and longitudinal. The modes A_1 and E_1 are in polar phonon mode and are divided into TO and LO. They are also active in Raman and IR. However, the E_2 mode is a non-polar phonon and active with Raman only, while the B_1 mode is Raman and the IR mode inactive [42].

CONCLUSIONS

Undoped and Cu-doped ZnO nanoparticles with wurtzite structure were successfully prepared by a hydrothermal method. Their structural and optical properties were studied using XRD, UV−Vis, Raman, and PL methods. XRD and Raman spectroscopy data indicated that Cu-doping does not change the ZnO wurtzite structure. The effect of Cu doping on particle size, structure and optical properties were also studied. XRD analysis reveals that the average particle size of pure ZnO is 13.50 nm. It decreased to 12.11 nm for the Cu−doped sample $Zn_{0.95}Cu_{0.05}O$, then to 11.00 nm when $x = 0.15$ ($Zn_{0.85}Cu_{0.15}O$). The photoluminescence study shows that the introduction of Cu into pure ZnO causes a decrease in surface defects, such as oxygen vacancies and zinc vacancies. The band gap decreased from 3.18 to 3.11 eV as the amount of Cu increases from $x = 0$ to 0.15. Cu doping influenced the ZnO band gap, which is important for solar cell and photocatalysis devices.

ACKNOWLEDGMENTS

REFERENCES

1. S. H. Ko, D. Lee, H. W. Kang, K. H. Nam, J. Y. Yeo, S. J. Hong, C. P. Grigoropoulos, and H. J. Sung, Nano Lett. **11**, 666 (2011).
2. M. Sathya, A. Claude, P. Govindasamy, and K. Sudha, Adv. Appl. Sci. Res. **3**, 2591 (2012).
3. K. Naeem and F. Ouyang, Phys. B **405**, 221 (2010).
4. M. Seo, Y. Jung, D. Lim, D. Cho, and Y. Jeong, Mater. Lett. **92**, 177 (2013).
5. O. V. Kibis and M. E. Portnoi, Phys. E (Amsterdam, Neth.) **40**, 1899 (2008).
6. A. Moulahi and F. Sediri, Mater. Res. Bull. **48**, 3723 (2013).
7. H. Morkoc, S. Strite, G. B. Gao, M. E. Lin, B. Sverdlov, and M. Burns, J. Appl. Phys. **76**, 1363 (1994).
8. U. Ozgur, Y. I. Alivov, C. Liu, A. Teke, M. A. Reshchikov, S. Dogan, V. Avrutin, S. J. Cho, and H. Morkoc, J. Appl. Phys. **98**, 041301 (2005).
9. D. C. Look, Mater. Sci. Eng. B **80**, 383 (2001).
10. K. Naeem and F. Ouyang, Phys. B (Amsterdam, Neth.) **405**, 221 (2010).
11. C. C. Chen, Ma. Wanhong, and J. C. Zha, Curr. Org. Chem. **14**, 630 (2010).
12. J. C. Sin, S. M. Lam, K. T. Lee, and A. R. Mohamed, Ceram. Int. **39**, 5833 (2013).
13. F. Kermiche, A. Taabouche, F. Hanini, S. Menakh, A. Bouabellou, Y. Bouachiba, T. Kerdja, Ch. Benazzouz, M. Bouafia, and S. Amara, Int. J. Neuropsychopharm. **6**, 93 (2013).
14. S. Karamat, R. S. Rawat, P. Lee, T. L. Tan, and R. V. Ramanujan, Proc. Nat. Sci. Mater. **24**, 142 (2014).
15. A. M. Ganose and D. O. Scanlon, J. Mater. Chem. C **4**, 1467 (2016).
16. X.-Y. Feng, Z. Wang, C.-W. Zhang, and P.-J. Wang, J. Nanomater. **2013**, 181979 (2013). https://doi.org/10.1155/2013/181979
17. A. Tsukazaki, M. Kubota, A. Ohtomo, T. Onuma, K. Ohtani, H. Ohno, Sh. F. Chichibu, and M. Kawasaki, Jpn. J. Appl. Phys. **44**, L643 (2005).
18. S. Sarkar and D. Basak, Appl. Phys. Lett. **103**, 041112 (2013).
19. H. Gong, J. Q. Hu, J. H. Wang, C. H. Ong, and F. R. Zhu, Sens. Actuators, B **115**, 247 (2006).
20. D. B. Buchholz, R. P. H. Chang, J. Y. Song, and J. B. Ketterson, Appl. Phys. Lett. **87**, 082504 (2005).
21. G. Z. Xing, J. B. Yi, J. G. Tao, T. Liu, L. M. Wong, Z. Zhang, G. P. Li, S. J. Wang, J. Ding, C. Sum, C. H. A. Huan, and T. Wu, Adv. Mater. **20**, 3521 (2008).
22. A. R. Kim, J.-Y. Lee, B. R. Jang, J. Y. Lee, H. S. Kim, and N. W. Jang, J. Nanosci. Nanotechnol. **11**, 6395 (2011).
23. S. Kumar, B. Koo, C. Lee, S. Gautam, K. Chae, S. Sharma, and M. Knobel, Funct. Mater. Lett. **4**, 17 (2011).
24. G. Rey, A. Redinger, J. Sendler, T. P. Weiss, M. Thevenin, M. Guennou, B. El Adib, and S. Siebentritt, Appl. Phys. Lett. **105**, 112106 (2014).
25. A. Moulahi and F. Sediri, Optics **127**, 7586 (2016).

26. S. Satheeskumar, V. Jeevanantham, and D. Tamilselvi, J. Ovonic Res. **14**, 9 (2018).

27. Z. Feng, Y. Wei, R. Liu, D. Yan, Y.-Ch. Wang, J. Luo, A. Senyshyn, C. Cruz, W. Yi, J.-W. Mei, Z. Y. Meng, Y. Shi, and S. Li, Phys. Rev. B **98**, 155127 (2018).

28. P. Labhane, V. Huse, L. Patle, A. Chaudhari, and G. Sonawane, J. Mater. Sci. Chem. Eng. **3**, 39 (2015).

29. J. Diouri, J. P. Lascaray, and M. El Amrani, Phys. Rev. B **31**, 7995 (1985).

30. R. B. Bylsma, W. M. Becker, J. Kossut, U. Debska, and D. Yoder-Short, Phys. Rev. B **33**, 8207 (1986).

31. I. Hamberg and C. G. Granqvist, J. Appl. Phys. **60**, R123 (1986).

32. C. Ton-That, M. Foley, and M. R. Phillips, Nanotechnology **19**, 415606 (2008).

33. C. Karunakaran, P. Gomathisankar, and G. Manikandan, Mater. Chem. Phys. **123**, 585 (2010).

34. A. Umar, B. Karunagaran, E. K. Suh, and Y. B. Hahn, Nanotechnology **17**, 4072 (2006).

35. S. T. Kuo, W. H. Tuan, J. Shieh, and S. F. Wang, J. Eur. Ceram. Soc. **27**, 4521 (2007).

36. R. S. Zeferino, M. B. Flores, and U. Pal, J. App. Phys. **109**, 014308 (2011).

37. L. Dai, X. L. Chen, W. J. Wang, T. Zhou, and B. Q. Hu, J. Phys.: Condens. Matter **15**, 2221 (2003).

38. K. A. Salman, K. Omar, and Z. Hassan, Sol. Energy **86**, 541 (2012).

39. A. Sharma, B. P. Singh, and S. Dhar, Surf. Sci. **606**, L13 (2012).

40. M. Šćepanovic, M. Grujić-Brojčin, K. Vojisavljević, S. Bernik, and T. Srećković, J. Raman Spectrosc. **41**, 914 (2010).

41. S. K. Panda and C. Jacob, Appl. Phys. A **96**, 805 (2009).

42. J. Marquina, Ch. Power, and J. González, Rev. Mex. Fis. **53**, 170 (2007).